

Article

Fatigue Properties of Ultra-Fine Grained Al-Mg-Si Wires with Enhanced Mechanical Strength and Electrical Conductivity

Andrey Medvedev ^{1,*}, Alexander Arutyunyan ², Ivan Lomakin ², Anton Bondarenko ², Vil Kazykhanov ¹, Nariman Enikeev ^{1,2}, Georgy Raab ¹ and Maxim Murashkin ^{1,2}

¹ Institute of Physics of Advanced Materials, Ufa State Aviation Technical University, 12 K. Marx st., 450008 Ufa, Russia; kvu08@yandex.ru (V.K.); nariman.enikeev@ugatu.su (N.E.); giraab@mail.ru (G.R.) m.murashkin.70@gmail.com (M.M.)

² Laboratory for Mechanics of Bulk Nanostructured Materials, Saint Petersburg State University, 199034 Saint-Petersburg, Russia; a.arutyunyan@spbu.ru (A.A.); ivan.v.lomakin@gmail.com (I.L.); bond.anton@gmail.com (A.B.)

* Correspondence: medvedevandreyrf@gmail.com; Tel.: +7-917-456-9074

Received: 9 November 2018; Accepted: 4 December 2018; Published: 6 December 2018



Abstract: This paper focuses on the mechanical properties, electrical conductivity and fatigue performance of ultra-fine-grained (UFG) Al-Mg-Si wires processed by a complex severe plastic deformation route. It is shown that the nanostructural design via equal channel angular pressing (ECAP) Conform followed by heat treatment and cold drawing leads to the combination of enhanced tensile strength, sufficient ductility, enhanced electrical conductivity, and improved fatigue strength compared to the wires after traditional T81 thermo-mechanical treatment used in wire manufacturing. The Processing-microstructure-properties relationship in the studied material is discussed.

Keywords: Al-Mg-Si alloy; severe plastic deformation; microstructure; strength; electrical conductivity; fatigue limit

1. Introduction

There has been a growing interest in the nanostructural design in Al alloys with the aim to achieve the combination of enhanced mechanical and functional properties therein. This has been typically done via processing by severe plastic deformation (SPD) followed by heat treatments [1–5]. Typically, SPD processing of the Al alloys results in the formation of an ultra-fine-grained (UFG) microstructure showing grain/subgrain size in the range of 50 nm to 1 μ m depending on the alloy composition and the applied thermo-mechanical path [1–5]. Earlier studies showed that grain refinement in the Al alloys down to the UFG scale may increase their mechanical strength by a factor of 1.2–2.0 compared to their coarse-grained (CG) counterparts processed by a standard aging treatment [1–4,6]. The Al alloys with UFG microstructure can also demonstrate improved ductility [1,7,8], fracture toughness [9] and electrical conductivity [1,10,11]. There have been significant research activities on fatigue performance of the UFG Al alloys which were overviewed in several manuscripts [12–17]. Their main conclusions can be shortly summarized as follows. The improvement of fatigue limit in the UFG Al alloys is not as high as the mechanical strength due to a low increase in resistance to fatigue crack nucleation in the high cycle fatigue (HCF) regime [13]. Reduced ductility of the UFG Al alloys results in very complex low cycle fatigue (LCF) behaviour due to fatigue crack initiation at the early stage and enhanced volume fraction of high angle grain boundaries promoting crack propagation. Low cycle hardening or even cyclic softening are typical for the UFG Al alloys deformed cyclically under constant strain

amplitude [18–20]. Manipulation of the nanostructural architecture in the Al alloys may improve their HCF and LCF behaviour [21,22].

The vast majority of experimental studies on fatigue behaviour of UFG Al alloys was carried out using samples processed mainly by equal-channel angular pressing (ECAP) [12–14], cryorolling [18,23] or high pressure torsion (HPT) [24]. However, in industrial manufacturing additional metal-forming operations have to be applied to the bulk UFG material in order to provide the final (or near-final) shape of the end product. The final metal-forming operations can dramatically modify the microstructure and thus, the properties of the material. Therefore, from the viewpoint of industrial end-users, the fatigue performance of the samples having a final (or near-final) shape similar to that of the end-product is of great importance. This paper studies the UFG Al-Mg-Si (Al6101) wires processed by ECAP-Conform followed by artificial aging and cold drawing (CD) as the final metal-forming operation in wire manufacturing. The properties of the UFG Al6101 are compared to its counterpart subjected to the standard T81 thermo-mechanical treatment used in wire manufacturing. The latter alloy has already been widely used in electrical engineering for overhead power lines, where strength, electrical conductivity and fatigue resistance play a key role [25]. Therefore, the main objective of the present work is to study fatigue properties taking into account also strength and electrical conductivity of the UFG Al 6101 wire in comparison with its commercial counterpart.

2. Materials and Methods

Commercial Al 6101 alloy in the T1 condition (cooled from an elevated temperature-shaping process and naturally aged) was selected as a material for study. Its chemical composition is: 0.58 Mg; 0.54 Si; 0.23 Fe; 0.003 Cu; 0.01 Zn; 0.012 (Σ Ti + V + Cr + Mn); res. Al (wt. %). The supplied material had a form of continuous cast re-draw rolled rods with a diameter of 12.5 mm. They were successively annealed at 550 °C, water quenched and subjected to SPD processing. To form the UFG structure, quenched billets were SPD-processed by ECAP-Conform technique for six passes under isothermal conditions at 130 °C. The intersection angle of channels (ψ) constituted 120°, resulting in an equivalent strain of about ~4 after six passes [26]. A wire rod was rotated around the axis by +90° after each ECAP-C cycle (route Bc). According to the previous studies [1,27,28], it is the most efficient mode to form a homogeneous UFG microstructure in the Al alloys. The ECAP-Conform processing resulted in rods having up to 1.5 m in length with a square cross-section of 11mm × 11 mm. No noticeable macro-defects were observed on their surface. The processed rods were artificially aged (AA) at 170 °C for 12h in order to achieve the optimal strength–conductivity balance [29]. Wire samples having a diameter of 3.2 mm after ECAP-C and AA were processed via cold drawing.

The T81 processed wires of the Al 6101 alloy were also studied for comparison. Currently, this is a standard processing route for the manufacturing of wires for application in the overhead power lines.

X-ray diffraction (XRD) studies were performed using Ultima IV diffractometer (Rigaku, Tokyo, Japan) by CuK α irradiation (30 kV and 20 mA). The size of coherent domains (D), values of mean-square microdistortion of crystalline lattice ($\langle \epsilon^2 \rangle^{1/2}$) and crystalline lattice parameter (a) were calculated using Rietveld analysis with the help of MAUD software (copyright by L. Lutterotti, Trento, Italy) [30]. To estimate dislocation density (ρ), Equation (1) was used [31].

$$\rho = 2\sqrt{3}\langle \epsilon^2 \rangle^{1/2} / Db \quad (1)$$

Microstructure characterization was performed by electron backscatter diffraction (EBSD) analysis using a scanning electron microscope Zeiss Merlin. The EBSD samples were prepared using conventional metallographic techniques followed by polishing using diamond and colloidal-silica suspensions. The EBSD mapping was performed on a scan area of 32.6 × 24.4 μm^2 with a scan step of 0.15 μm . At least 1000 grains were analysed for each studied material condition. Seven Kikuchi bands were used for indexing diffraction patterns. Distribution of grain sizes and grain boundaries misorientation angle θ were determined from the EBSD maps. GBs with $\theta < 15^\circ$ were referred to

as low-angle grain boundaries (LAGBs) and GBs with $\theta \geq 15^\circ$ were considered as high-angle grain boundaries (HAGBs).

Microstructure studies were also performed using the transmission electron microscope (TEM, JEOL, Tokyo, Japan) JEM 2100 at an accelerating voltage of 200 kV. Observations were made in both the bright and the dark field imaging modes, and selected area electron diffraction (SAED) patterns were recorded from the areas of interest using an aperture of $1\ \mu\text{m}$ nominal diameter. The linear intercept method was used to measure grain size. At least 200 grains were analyzed to estimate the average grain size.

The electrical resistivity of the studied material was measured in accordance with the IEC 60468:1974 standard (CEN, Bruxelles, Belgium) [32]. Straightened samples of at least 1 m long in a rectified part were taken.

Cylindrical tensile specimens having a gauge length of 15 mm and gauge diameter of 3 mm were machined from the rods before and after ECAP-C processing. Wire samples after ECAP-C and AA followed by cold drawing, as well as after T81, have 250 mm gauge length. Mechanical tensile tests were performed at room temperature using Instron 5982 tensile testing machine with a strain rate of $10^{-3}\ \text{s}^{-1}$. Yield strength ($\sigma_{0.2}$), ultimate tensile strength (σ_{UTS}) and elongation to failure (δ) were estimated from the recorded engineering stress-engineering strain curves. To obtain consistent results, at least three samples were tested per each data point, and the results were found to be reproducible.

Fatigue limit was measured for the SPD processed and T81 processed alloys. High cycle fatigue tests were carried out on specimens having similar geometry (a gauge length of 15 mm and gauge diameter of 3 mm) and in the repeated stress loading condition, where the stress varied between zero and the maximum tensile stress σ_{max} in a cyclic manner. The stress ratio $R = \sigma_{\text{min}}/\sigma_{\text{max}} = 0$, and the stress amplitude was $\sigma_{\text{amp}} = \sigma_{\text{max}}/2$. The testing frequency was 50 Hz. The value of stress amplitude was in the range of 70–200 MPa for both tested conditions. At least three specimens were tested for each stress amplitude. The number of cycles before specimen failure was counted, and the S-N curves (Woehler curves) were plotted based on the obtained results. The fatigue limit was determined as the number of cycles of 10^7 .

3. Results and Discussion

3.1. Effect of Complex SPD Processing on Microstructure

Figure 1 illustrates the EBSD map of the microstructure of the alloy after solution treatment before SPD processing. An inhomogeneous microstructure consisting of elongated coarse grains having a width of 10 to 50 μm and finer spherical grains having a size of 1 to 5 μm is observed. Such a microstructure is typical for the aluminium alloys produced by rolling.

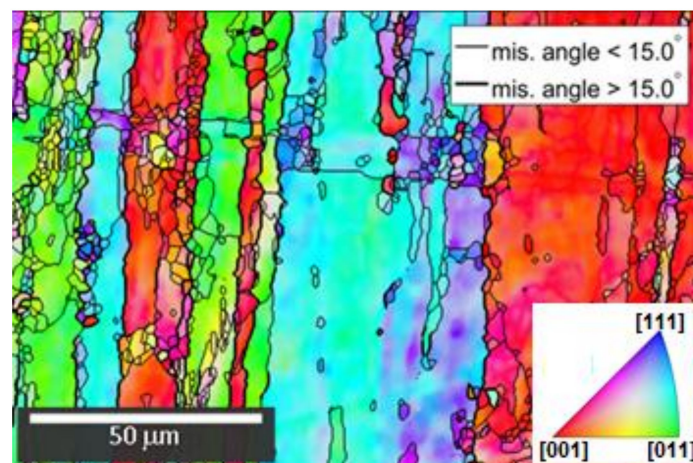


Figure 1. EBSD orientation map of the alloy after solution heat treatment.

ECAP-Conform processing results in significant grain refinement and the formation of a homogeneous microstructure with a significant fraction of ultra-fine grains (Figure 2). Low angle grain boundaries dominate in the microstructure. As seen from the histogram of grain boundary misorientation distribution (Figure 2e), their fraction exceeds 50%. The average grain size of 1.7 μm (Figure 2f) can be determined from the histogram of grain size distribution. TEM analysis indicates that grain boundaries are well-defined, and dislocation tangles can be noticed on the TEM images (Figure 2a,b). The X-ray measurements show an average dislocation density of $8 \times 10^{13} \text{ m}^{-2}$ in the material after ECAP-C processing, which is relatively low compared to the SPD processed Al alloys [1] and relevant to that of the Al6101 alloy after conventional T81 treatment ($9.5 \times 10^{13} \text{ m}^{-2}$) (Table 1).

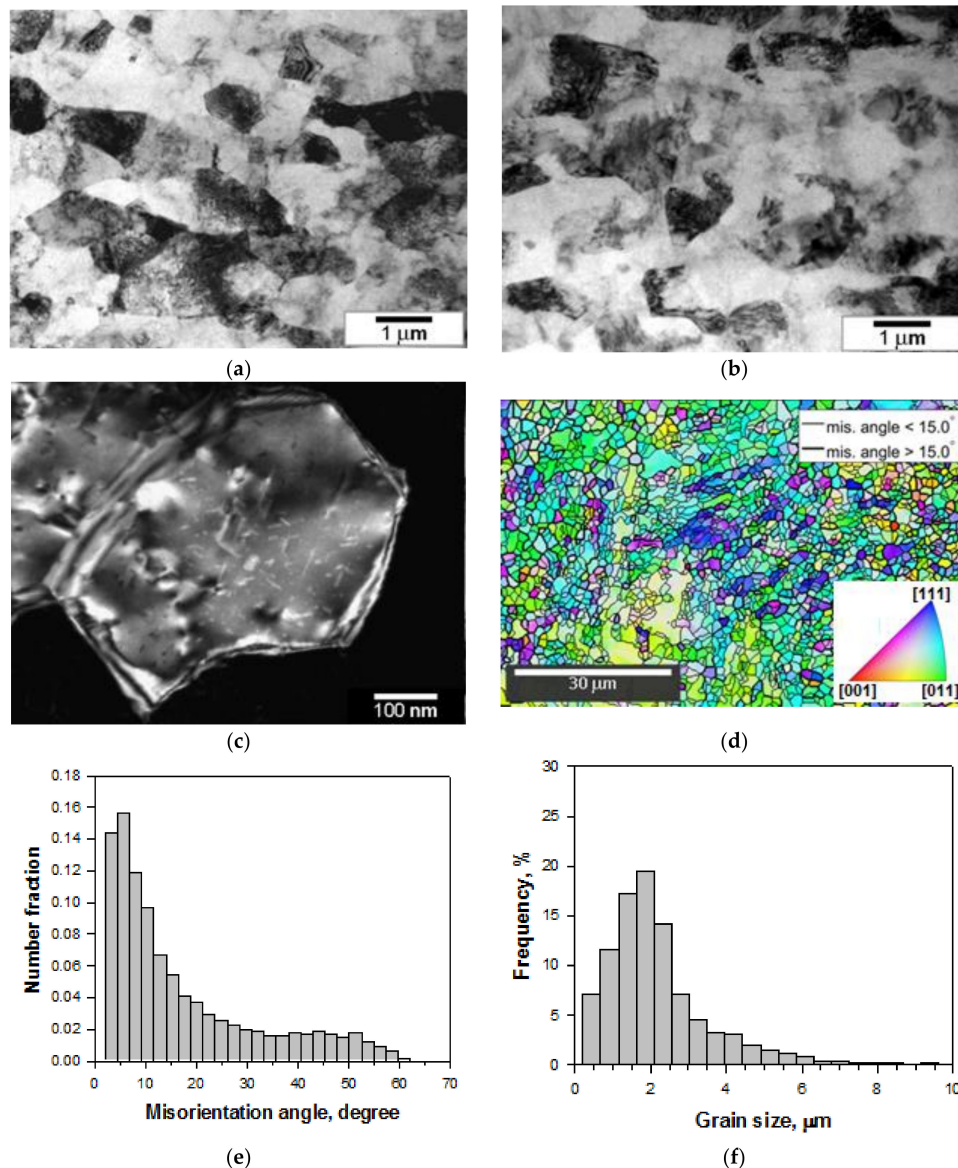


Figure 2. Al 6101 alloy after ECAP-C and AA at 170°C. (a,c) TEM images in the longitudinal section; (b) TEM image in the cross section; (d) EBSD map, cross section; (e) misorientation distributions, obtained from the cross section; (f) grain size distributions, obtained from the cross section.

This can be related to the ECAP-C processing at the elevated temperature resulting in recovery. Further artificial aging reduces it down to $4.3 \times 10^{13} \text{ m}^{-2}$. Formation of the rod-shaped metastable β' -nanoprecipitates in the grain interior during artificial aging can also be clearly seen on the TEM images (Figure 2c). Such precipitates are typically formed during artificial aging of the Al-Mg-Si

alloys [10,11,29,33]. It should be noted that the size of the coherently scattered domain (CSD) measured by XRD (Table 1) is by an order of magnitude lower compared to the grain/subgrain size observed in TEM and EBSD analysis (Figure 2). As it is well known, the CSD size measured by XRD typically yields much lower values of grain or subgrain size in the SPD processed metallic materials. This observation was earlier rationalized based on the contribution of dipolar dislocation walls without differences in the orientation, which break down the coherency of X-ray scattering [34].

Table 1. Results of the X-ray diffraction analysis of the Al 6101 alloy.

State/Treatment	D_{hkl} , [nm]	$\langle \varepsilon^2 \rangle^{1/2}$, [%]	a , [Å]	ρ , [m^{-2}]
Initial state—T1 (this work)	-	-	4.0531 ± 0.0008	-
6 cycles ECAP-Cat 130 °C	165 ± 20	0.110 ± 0.024	4.0520 ± 0.0002	8.0×10^{13}
ECAP-C + AAat 170 °C	188 ± 13	0.067 ± 0.031	4.0508 ± 0.0004	4.3×10^{13}
ECAP-C + AA + CD	84 ± 1	0.097 ± 0.008	4.0507 ± 0.0003	1.4×10^{14}
Conventional TMT T81	81 ± 4	0.054 ± 0.005	4.0516 ± 0.0002	9.5×10^{13}

CD results in the formation of fiber-type grains elongated along the drawing axis and having a width of 200–300 nm (Figure 3a). TEM analysis of the transversal section of the cold drawn wires shows equiaxed grains with the same range of size (Figure 3b). Individual dislocations are also seen in the interior of grains and at grain boundaries. The XRD measurements yield a dislocation density of $1.4 \times 10^{14} m^{-2}$, which is very close to that in the conventionally processed Al 6101 alloy (Table 1). The CD leads to spheroidization of the rod-shaped second phase nanoprecipitates, which could be related to the shearing of rod-shaped precipitates by gliding dislocations during CD (Figure 3c,d). They have a diameter in the range of 5–15 nm. Similar observations were reported earlier for other Al-Mg-Si alloys in Reference [34].

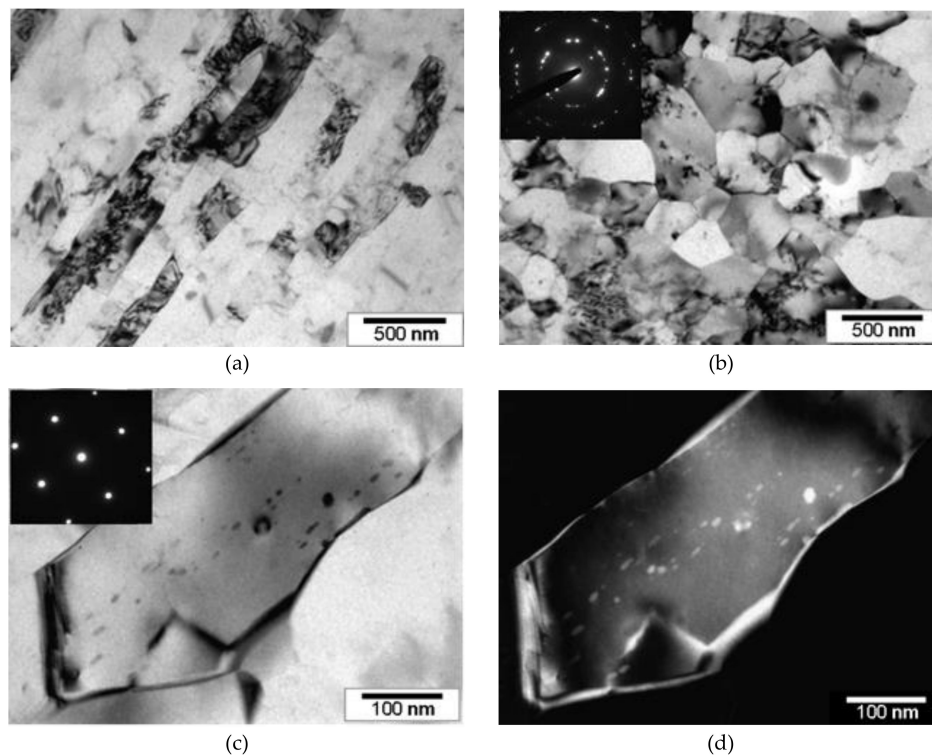


Figure 3. The Al 6101 alloy after ECAP-C processing, artificial aging and CD: (a,c,d) microstructure on longitudinal section; (b) transversal section and corresponding SAED patterns; (c) bright field TEM image and corresponding SAED patterns (the crystal is close to the [001] zone axis orientation); and (d) dark field TEM image showing spherical second-phase nanoprecipitates present in the Al matrix, TEM.

Figure 4 presents TEM images of the microstructure of the conventional thermo-mechanically (T81) processed Al 6101 alloy. Its microstructure is distinctly different from the microstructure of the ECAP-C processed alloy after artificial aging and CD. First, the width of the elongated grains in the T81 processed alloy are higher and reach about $0.4\ \mu\text{m}$ (Figure 4a). Second, the needle-type metastable β'' -nanoprecipitates are present in the microstructure (Figure 4c,d). This difference is also clearly seen from the outcomes of the EBSD characterization of these materials' conditions (Figure 5). The EBSD results indicate that the average grain width in the T81 processed alloys is about $1\ \mu\text{m}$ (Figure 5g), whereas its SPD processed counterpart demonstrates a very homogeneous microstructure with the average grain size of $0.4\ \mu\text{m}$ (Figure 5h). It should also be noted that the T81 processed alloy has a heterogeneous microstructure (Figure 5a,c), and coarser grains having a size up to $4\ \mu\text{m}$ (Figure 5h) occupy a significant fraction of the microstructure in the T81 processed alloy. Moreover, the fraction of HAGBs in the T81 processed alloy (49%) is much lower compared to that in the SPD processed material (70%).

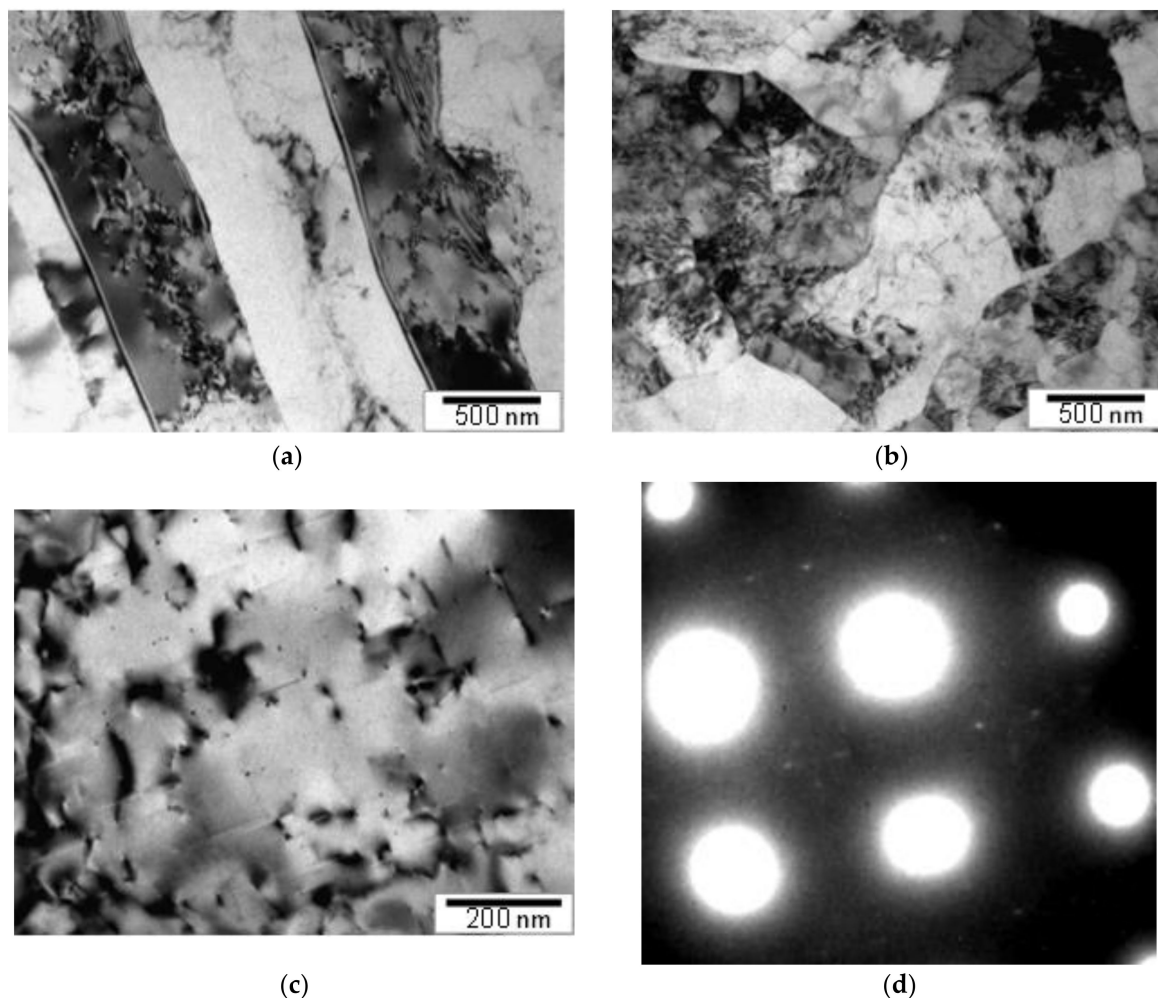
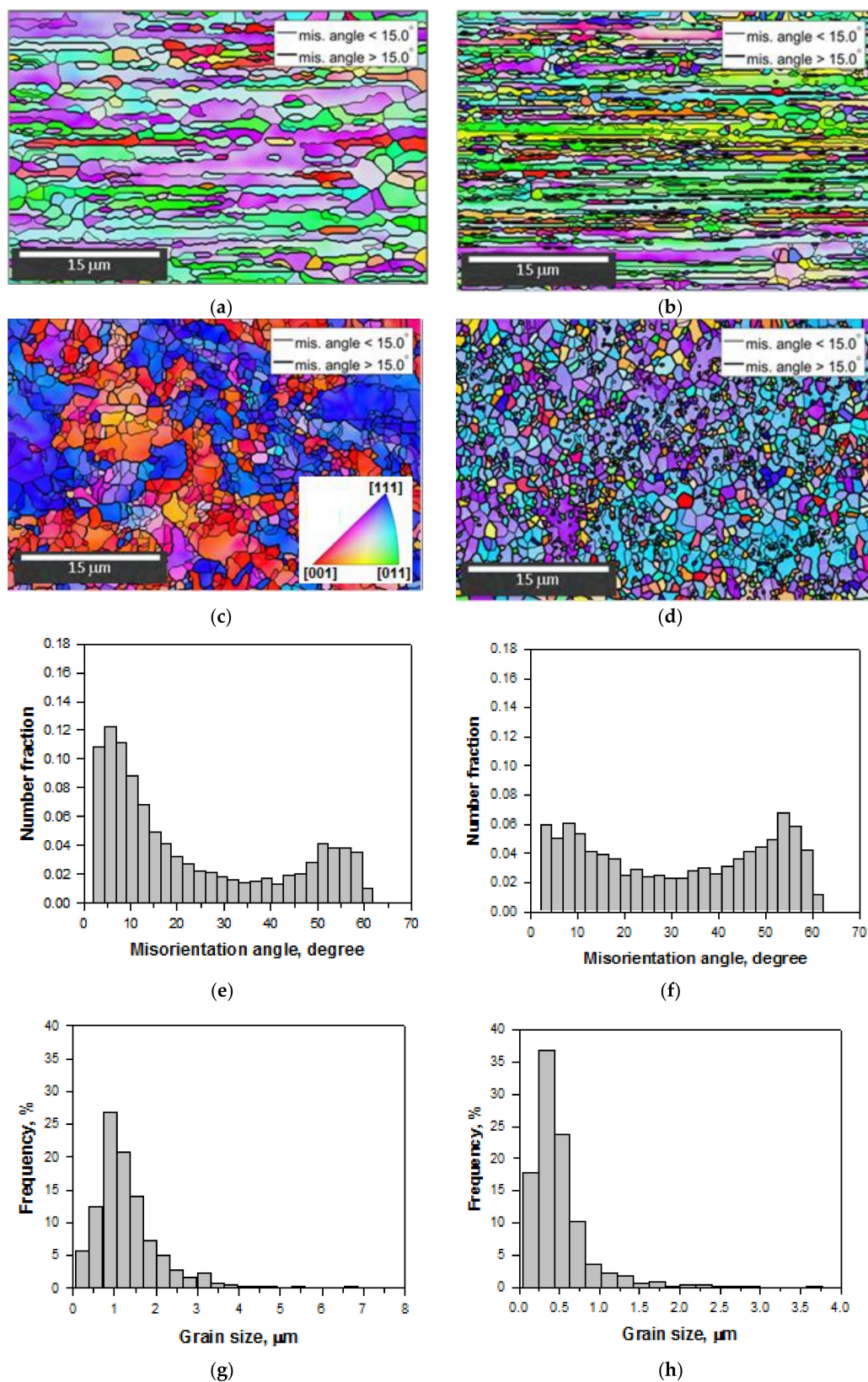


Figure 4. The Al 6101 alloy after conventional thermo-mechanical treatment T81: (a) microstructure on longitudinal section; (b) microstructure on transversal section; (c) bright field TEM image showing strengthening second-phase precipitates present in the Al matrix; and (d) corresponding SAED patterns (the crystal is close to the $[001]$ zone axis orientation), TEM.



3.2. Effect of SPD Processing on Electrical Conductivity of the Wires

Outcomes of the electrical conductivity measurements are presented in Table 2. The evolution of electrical conductivity during SPD processing of the alloy can be analyzed. The ECAP-C processing at 130 °C results in an increase of electrical conductivity from 50.4% to 53.2% of IACS (International Annealed Copper Standard). This is related to the homogenization of the microstructure and dynamic aging during ECAP-C processing [29] compared to the T1 condition, when the material is cooled from an elevated temperature and naturally aged. The artificial aging of the ECAP-C processed material results in a further increase of electrical conductivity to 57.1% of IACS, which is due to the purification of the matrix from the Mg and Si solute atoms via nanoprecipitation. As it is well known, the conducting electrons are most effectively scattered at the solute atoms, while their scatter at the second phase precipitates is less intensive [11]. Decomposition of supersaturated solid solution and formation of nanoprecipitates leads to improved electrical conductivity in the material [11]. Further CD of the artificially-aged alloy results in a slight reduction of electrical conductivity to 56.4% of IACS due to an increase in dislocation density detected by the XRD measurements (Table 1). The lattice defects are also known to scatter the conducting electrons, although at a lower extent than the solute atoms [11]. Nevertheless, the electrical conductivity of the SPD processed wires is much higher compared to that measured in the T81 conventionally processed alloy (54.1% of IACS). This can be related mainly to a higher degree of purification of the Al matrix from Mg and Si atoms, demonstrated by shifting the lattice parameter towards a pure aluminium value (Table 1), and the needle-type metastable nanoprecipitates in the microstructure of the latter material (Figure 4). As it is well known, the conducting electrons are scattered more effectively at the needle-type precipitates than at the spherical precipitates, respectively [11,35].

Table 2. Mechanical properties and electrical conductivity of the Al 61 01 alloy during processing.

State/Treatment	$\sigma_{0.2}$ [MPa]	σ_{UTS} [MPa]	δ [%]	Resistivity [nΩm]	IACS [%]	σ_R [MPa]	σ_R/σ_{UTS}	Ref.
Initial state—T1 ¹	120 ± 1	195 ± 2	22.4 ± 0.4	34.23	50.4	-	-	
6 cycles ECAP-C at 130 °C	282 ± 8	308 ± 9	15.1 ± 0.6	32.42	53.2	-	-	[29]
ECAP-C + AA at 170 °C	291 ± 10	304 ± 3	15.0 ± 2	30.20	57.1	-	-	
ECAP-C + AA + CD	-	364 ± 9	3.5 ± 0.2	30.55	56.4	100	0.27	This work
Convention T81	-	309 ± 7	4.1 ± 0.3	31.87	54.1	80	0.26	

¹ State of type T1—Cooled from an elevated temperature shaping process and naturally aged.

3.3. Effect of Complex SPD Processing on the Mechanical Properties and Fatigue Resistance

The results of mechanical tensile testing of the Al 6101 alloy after the conventional T81 treatment and evolution of mechanical properties during processing via complex SPD route are presented in Table 2. It is seen that the ECAP-C processing dramatically increases the mechanical strength of the alloy. Yield strength increases by a factor of ~2.5 and its ultimate tensile strength increases by a factor of ~1.5, while its ductility somewhat decreases from 22.4% to 15.1%. Surprisingly, artificial aging of the alloy affects neither its mechanical strength nor its ductility, while it is well known that precipitation hardening during artificial aging of the Al alloys typically improves their strength [33]. It can be hypothesized that the strengthening effect due to the precipitation (Figure 3) is compensated by the softening effect due to the reduction of dislocation density via recovery resulting in no noticeable change of the mechanical properties (Table 1). CD of the artificially-aged material further increases its ultimate tensile strength to 364 MPa at the expense of its ductility, which is dramatically reduced from 15% to 3.5%. Such a significant increase of mechanical strength by 60 MPa can be rationalized based on the additional grain refinement during the CD process (Figure 3) and an increase of dislocation density (Table 1). It should be noted that the T81 processed alloy shows much lower mechanical strength (309 MPa) at the same level of ductility (4.1%) (Table 2). This is also clearly seen from the engineering

stress–engineering strain curves presented in Figure 6a. The lower strength of the T81 processed alloy is due to coarser grains reducing the grain-size-hardening effect [1,11,12] (Figure 5).

Cyclic tests yield a fatigue limit of 100 MPa for the SPD processed alloy, while its traditionally T81 processed counterpart showed a lower fatigue limit of 80 MPa (Figure 6b, Table 2). The enhanced fatigue strength of the SPD processed alloy can be entirely related to its higher mechanical strength. Indeed, the σ_R/σ_{UTS} ratio for both materials has very similar values: 0.27 for the SPD processed material and 0.26 for the T81 processed one (Table 2).

It should be noted that a somewhat higher level of the σ_R/σ_{UTS} ratio (0.30) was reported earlier for the high-pressure torsion-processed Al 6061 alloy with a grain size of 170 nm in Reference [24], while a lower σ_R/σ_{UTS} ratio of 0.20 was reported for the UFG Al 6061 alloy with an average grain size of 0.6 μm processed by ECAP in Reference [21]. Such low σ_R/σ_{UTS} ratios were found also in other ECAP-processed Al-Mg-Si alloys [12,13]. It is hard to make a direct conclusion about the effect of grain size on the σ_R/σ_{UTS} ratio in the considered UFG Al-Mg-Si alloys, as the ECAP and HPT processed alloys had equiaxed grains, while the Al 6101 alloys studied in the present work had fiber-type grains. Nevertheless, it can be assumed that the amount of dislocations gliding across the elongated grain is much higher compared to the number of dislocations gliding along the elongated grain. Therefore, the width of elongated grains can be taken as a measure of grain size for the SPD and T81 processed alloys. A trend for increasing the σ_R/σ_{UTS} ratio with decreasing grain size can be outlined. Therefore, it can be hypothesized that dramatic grain refinement close to the nanoscale (i.e., 100 nm) in the Al-Mg-Si alloys improves the fatigue limit not only due to the enhanced tensile strength. As it is well known, the fatigue life of the metallic materials during HCF is controlled by fatigue crack initiation [36]. Therefore, the enhanced resistance to the fatigue crack initiation with decreasing grain size could be another factor improving the fatigue limit of the Al-Mg-Si alloys.

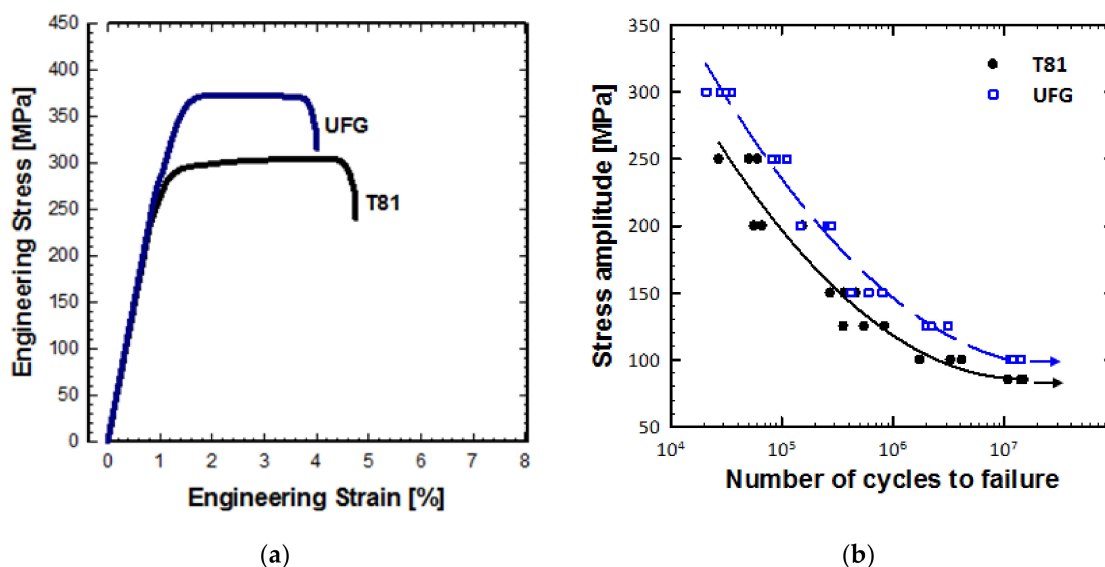


Figure 6. Engineering stress–engineering strain curve (a) and fatigue curves (S-N curves) (b) for the alloy after ECAP-C processing followed by artificial aging, cold drawing (referred to as UFG) and conventional T81 processing (referred to as T81).

3.4. About Potential Application of the Developed Processing Route

The outcomes of this investigation clearly demonstrate that the microstructural design in the commercial Al 6101 alloy via complex processing through combination of the SPD method, artificial aging and metal-forming operation can lead to a set of simultaneously improved properties, such as strength, electrical conductivity and fatigue limit, and retaining ductility at the level sufficient for stranding of wires [1]. These are the key properties from the viewpoint of the manufacturing and service life of overhead power lines. Enhanced electrical conductivity will dramatically reduce the

power loss in transmission lines, whereas the enhanced mechanical strength along with the improved fatigue limit would allow for increasing the distance between neighbor fermas of the overhead power lines [25]. The developed processing technology opens new avenues for the manufacturing of advanced wires for the modern electrical engineering.

4. Conclusions

The evolution of microstructure, tensile mechanical properties, electrical conductivity, and fatigue limit of the Al 6101 wires during processing by complex severe plastic deformation route were studied. The microstructure and properties were compared with those of the conventional T81 processed Al 6101 wire. The effect of processing on the microstructure and mechanical properties was analysed. The following conclusions can be drawn.

1. The ECAP-C processing for six passes at 130 °C results in significant grain refinement and formation of the homogeneous microstructure with an average grain size of 1.7 μm , a significant fraction of ultra-fine grains and dominating low angle grain boundaries. Artificial aging at 170 °C for 10 h leads to the formation of rod-shaped metastable β' -nanoprecipitates in the grain interior and reduction of dislocation density. Final CD results in the formation of fiber-type grains elongated along the drawing axis, having a width of 200–300 nm with spherical nano-precipitates and dominating high angle grain boundaries. The microstructure of the T81 processed alloy is characterized by coarser fiber-type grains (about 1 μm) and needle-type metastable β'' -nanoprecipitates.
2. The ECAP-C processing of the alloy increases its electrical conductivity, which is further enhanced during artificial aging due to the purification of the Al matrix from solute atoms. Despite a slight reduction of electrical conductivity after CD, the SPD processed wire still demonstrates significantly higher electrical conductivity compared to the conventional T81 processed Al 6101 commercial alloy.
3. The SPD processed Al 6101 wire shows significantly higher mechanical strength and fatigue resistance (by ~20%) and similar levels of ductility compared to the conventional T81 processed counterpart.
4. The improved combination of mechanical strength, fatigue resistance and electrical conductivity of the SPD processed Al 6101 wire in comparison with the T81 processed one is related to the finer grain size and spherical β' -nanoprecipitates. Commercialization of the developed technology for manufacturing of UFG wires could lead to a significant reduction of energy loss in the transmission of overhead power lines. Another benefit is related to the lower cost of construction and the service of the power lines due to larger spacing between fermas.

Author Contributions: A.M. supervised the workflow and created the initial draft, carried out mechanical tensile tests, conductivity measurements. A.A. provided fatigue tests. I.L. carried out mechanical tensile tests. A.B. performed microstructural characterization of the processed material by EBSD. V.K. performed microstructural characterization studies of the processed material by TEM. N.E. performed microstructural characterization with the help of the X-ray diffraction analysis. G.R. processed the wire rods by ECAP-C and cold drawing, as well as wire rods after T81 treatment. M.M. formulated the idea of this work, contributed with the overall supervision and development of the main concepts presented in this paper. All authors discussed the experimental results, participated in manuscript preparation and approved the final manuscript.

Funding: M. Murashkin, A. Arutyunyan and I. Lomakin would like to thank the Russian Science Foundation for financial support of this research by project No. 17-19-01311.

Acknowledgments: EBSD analysis was performed at the Research Park of St. Petersburg State University Interdisciplinary Center for Nanotechnology.

Conflicts of Interest: The authors declare no conflict of interest.

References

1. Valiev, R.Z.; Zhilyaev, A.P.; Langdon, T.G. *Bulk Nanostructured Materials: Fundamentals and Applications*; John Wiley & Sons: Hoboken, NJ, USA, 2014; p. 456.
2. Sabirov, I.; Murashkin, M.Y.; Valiev, R.Z. Nanostructured aluminium alloys produced by severe plastic deformation: New horizons in development. *Mater. Sci. Eng. A* **2013**, *560*, 1–24. [[CrossRef](#)]
3. Markushev, M.V.; Murashkin, M.Y. Mechanical properties of submicrocrystalline Al alloys processed by equal-channel angular pressing. *Phys. Met. Metall.* **2000**, *90*, 506–515.
4. Roven, H.J.; Nesboe, H.; Werenskiold, J.C.; Seibert, T. Mechanical properties of aluminum alloys processed by SPD: Comparison of different alloy systems and possible product areas. *Mater. Sci. Eng. A* **2005**, *410–411*, 426–429. [[CrossRef](#)]
5. Lyakishev, N.P.; Alymov, M.I.; Dobatkin, S.V. Structural bulk nanomaterials. *Russ. Metall.* **2003**, *3*, 191–202.
6. Dobatkin, S.V.; Zakharov, V.V.; Vinogradov, A.Y.; Kitagawa, N.; Krasilnikov, N.A.; Rostova, T.D.; Bastrash, E.N. Nanocrystalline structure in Al-Mg-Sc alloys by severe plastic deformation. *Russ. Metall.* **2006**, *6*, 533–540. [[CrossRef](#)]
7. Zhao, Y.; Liao, X.; Cheng, S.; Ma, E.; Zhu, Y. Simultaneously increasing the ductility and strength of nanostructured alloys. *Adv. Mater.* **2006**, *18*, 2280–2283. [[CrossRef](#)]
8. Horita, Z.; Ohashi, K.; Fujita, T.; Kaneko, K.; Langdon, T.G. Achieving high strength and high ductility in precipitation-hardened alloys. *Adv. Mater.* **2005**, *17*, 1599–1603. [[CrossRef](#)]
9. Markushev, M.V.; Bampton, C.C.; Murashkin, M.Y.; Hardwick, D.A. Structure and properties of ultra-fine grained Al alloys produced by severe plastic deformation. *Mater. Sci. Eng. A* **1997**, *234–236*, 927–931. [[CrossRef](#)]
10. Murashkin, M.; Sabirov, I.; Kazykhanov, V.; Bobruk, E.; Dubravina, A.; Valiev, R.Z. Enhanced mechanical properties and electrical conductivity in ultra-fine grained Al alloy processed via ECAP-PC. *J. Mater. Sci.* **2013**, *48*, 4501–4509.
11. Valiev, R.Z.; Murashkin, M.Y.; Sabirov, I. A nanostructural design to produce high-strength Al alloys with enhanced electrical conductivity. *Scr. Mater.* **2014**, *76*, 13–16. [[CrossRef](#)]
12. Vinogradov, A.Y.; Khasimoto, S. Fatigue in ultrafine-grained materials processed by equal-channel angular pressing. *Russ. Metall.* **2004**, *1*, 42–51.
13. Estrin, Y.; Vinogradov, A. Fatigue behaviour of light alloys with ultrafine grain structure produced by severe plastic deformation: An overview. *Int. J. Fatigue* **2010**, *32*, 898–907. [[CrossRef](#)]
14. Estrin, Y.; Vinogradov, A. Extreme grain refinement by severe plastic deformation: A wealth of challenging science. *Acta Mater.* **2013**, *61*, 782–817. [[CrossRef](#)]
15. Höppel, W.; Kautz, M.; Murashkin, M.Y.; Xu, C.; Langdon, T.G.; Valiev, R.Z.; Mughrabi, H. An overview: Fatigue Behavior of Ultrafine-Grained Metals and Alloys. *Int. J. Fatigue* **2006**, *28*, 1001–1010. [[CrossRef](#)]
16. Höpel, H.W.; Göken, M. Fatigue Behavior in Nanostructured Metals. In *Nanostructured Metals and Alloys: Processing, Microstructure, Mechanical Properties and Applications*; Whang, S.H., Ed.; Woodhead Publishing Limited: Suite, PA, USA, 2011; pp. 507–541.
17. Mughrabi, H.; Höppel, H.W.; Kautz, M. Fatigue and microstructure of ultra-fine grained metals produced by severe plastic deformation. *Scr. Mater.* **2004**, *51*, 807–812. [[CrossRef](#)]
18. Malekjani, S.; Hodgson, P.D.; Cizek, P.; Sabirov, I.; Hilditch, T.B. Cyclic deformation response of UFG 2024 Al alloy. *Int. J. Fatigue* **2011**, *33*, 700–709. [[CrossRef](#)]
19. Canadinc, D.; Maier, H.J.; Gabor, P.; May, J. On the cyclic deformation response of ultrafine-grained Al-Mg alloys at elevated temperatures. *Mater. Sci. Eng. A* **2008**, *496*, 114–120. [[CrossRef](#)]
20. Vinogradov, A.; Washikita, A.; Kitagawa, K.; Kopylov, V.I. Fatigue life of fine-grain Al-Mg-Sc alloys produced by equal-channel angular pressing. *Mater. Sci. Eng. A* **2003**, *349*, 318–326. [[CrossRef](#)]
21. Chung, C.S.; Kim, J.K.; Kim, H.K.; Kim, W.J. Improvement of high-cycle fatigue life in a 6061 Al alloy produced by equal channel angular pressing. *Mater. Sci. Eng. A* **2002**, *337*, 39–44. [[CrossRef](#)]
22. Lapovok, R.; Loader, C.; Dalla Torre, F.H.; Semiatin, S.L. Microstructure evolution and fatigue behavior of 2124 aluminum processed by ECAE with back pressure. *Mater. Sci. Eng. A* **2006**, *425*, 36–46. [[CrossRef](#)]
23. Malekjani, S.; Hodgson, P.D.; Cizek, P.; Hilditch, T.B. Cyclic deformation response of ultra-fine pure Al. *Acta Mater.* **2011**, *59*, 5358–5367. [[CrossRef](#)]

24. Murashkin, M.; Sabirov, I.; Prosvirnin, D.; Ovid'ko, I.; Terentiev, V.; Valiev, R.; Dobatkin, S. Fatigue behavior of an ultrafine-grained Al-Mg-Si alloy processed by high-pressure torsion. *Metals* **2015**, *5*, 578–590. [[CrossRef](#)]
25. Kiessling, F.; Nefzger, P.; Nolasco, J.F.; Kaintzyk, U. *Overhead Power Lines: Planning, Design, Construction*; Springer: Berlin, Germany, 2003.
26. Segal, V.M. Materials processing by simple shear. *Mater. Sci. Eng. A* **1995**, *147*, 157–164. [[CrossRef](#)]
27. Raab, G.J.; Valiev, R.Z.; Lowe, T.C.; Zhu, Y.T. Continuous processing of ultrafine grained Al by ECAP-Conform. *Mater. Sci. Eng. A* **2004**, *382*, 30–34. [[CrossRef](#)]
28. Valiev, R.Z.; Langdon, T.G. Principles of equal-channel angular pressing as a processing tool for grain refinement. *Prog. Mater. Sci.* **2006**, *51*, 881–981. [[CrossRef](#)]
29. Murashkin, M.; Medvedev, A.; Kazykhanov, V.; Krokhin, A.; Raab, G.; Enikeev, N.; Valiev, R.Z. Enhanced Mechanical Properties and Electrical Conductivity in Ultrafine-Grained Al 6101 Alloy Processed via ECAP-Conform. *Metals* **2015**, *5*, 2148–2164. [[CrossRef](#)]
30. Lutterotti, M.; Matthies, S.; Wenk, H.R. MAUD (Material Analysis Using Diffraction): A user friendly Java program for Rietveld Texture Analysis and more. In Proceeding of the 12th International Conference on Textures of Materials (ICOTOM-12), Montreal, QC, Canada, 9–13 August 1999; p. 1599.
31. Williamson, L.K.; Smallman, R.E. III. Dislocation densities in some annealed and cold-worked metals from measurements on the X-ray Debye-Scherrer spectrum. *Philos. Mag.* **1956**, *1*, 34–45. [[CrossRef](#)]
32. International Electrotechnical Commission (IEC). *IEC 60468: Method of Measurement of Resistivity of Metallic Materials*; IEC: Geneva, Switzerland, 1974.
33. Mondolfo, L.F. *Aluminum Alloys: Structure and Properties*; Butterworth: Oxford, UK, 1976; p. 971.
34. Ungar, T.; Tichy, G.; Gubicza, J.; Hellmig, R.J. Correlation between subgrains and coherently scattering domains. *Powder Diffr.* **2005**, *20*, 366–376. [[CrossRef](#)]
35. Rositter, P.L. *The Electrical Resistivity of Metals and Alloys*; Cambridge University Press: Cambridge, UK, 2003.
36. Suresh, S. *Fatigue of Materials*; Cambridge University Press: Cambridge, UK, 1998; p. 679.



© 2018 by the authors. Licensee MDPI, Basel, Switzerland. This article is an open access article distributed under the terms and conditions of the Creative Commons Attribution (CC BY) license (<http://creativecommons.org/licenses/by/4.0/>).